Available online at www.sciencedirect.com
SCIENCE DIRECT®
International Journal of Heat and Mass Transfer 48 (2005) 5270–5283
International Journal of HEAT and MASS TRANSFER
www.elsevier.com/locate/ijhmt

Sharp interface simulation of interaction of a growing dendrite with a stationary solid particle

Yi Yang, J.W. Garvin, H.S. Udaykumar *

Department of Mechanical and Industrial Engineering, University of Iowa, 3026 Seamans Center, Iowa City, IA 52242-1527, United States

Received 4 April 2005; received in revised form 20 July 2005
Available online 29 September 2005

Abstract

Numerical simulations are performed to study the response of a dendrite as it approaches a solid particle in the melt, such as may arise in metal-matrix composite solidification. A sharp interface, fixed grid numerical method is employed. A pure under-cooled melt is used to grow the dendrite. When the dendrite approaches the particle, appropriate interfacial conditions are specified at the particle-solid interface before and after contact. The behaviour of dendrites as they approach and grow around the particle is closely examined. For a particle to melt thermal conductivity ratio $\lambda = \frac{k_p}{k_l} < 1$ corresponding to the situation for metal-matrix composites, for the parameters employed, the solidification front does not approach close enough to the particle to activate the particle pushing mechanism. Instead, the solidification front chooses to go around the particle, and eventually the particle is engulfed by sidebranches. Thus an entrapment mode of front-particle interaction is the likely outcome under dendritic growth conditions for $\lambda < 1$.

1. Introduction

The interaction between a particle and a solid–liquid interface is important in many applications, particularly in the processing of metal matrix composites (MMC). A particle will do one of three things when a (planar) freezing front approaches it: (1) it will be pushed along with the moving front, (2) be engulfed in the front instantaneously, or (3) it will be pushed followed by engulfment [1,2]. When a particle is approached by an advancing solidification front, the solidification front must obtain a certain "critical velocity" in order to engulf the particle, as first observed by Uhlmann et al. [3]. If the solidification velocity is below this critical value, the particle will be pushed, and if the front velocity is above this value, then the particle will be engulfed. When it is approached by the front, the particle will experience both repulsive forces, pushing the particle away from the front, and attractive forces, pushing the particle towards the front. The nature of these forces varies depending on the model. An overview of the different models is given by Asthana et al. [4] (see also [5,6]). These differences arise from different models adopted for the drag (the forces that pushes the particle towards the interface) and the interfacial force (the force that pushes it away from the interface).

* Corresponding author. Tel.: +1 319 384 0832; fax: +1 319 335 5669.
E-mail address: ush@icaen.uiowa.edu (H.S. Udaykumar).

0017-9310/$ - see front matter © 2005 Elsevier Ltd. All rights reserved.
doi:10.1016/j.ijheatmasstransfer.2005.07.028

Almost all of the theory on particle-front interaction has relied on the fate of the particle in the following scenario:

1. The particle is approached by a planar solidification front with a constant, well-controlled velocity (i.e. the material is being directionally solidified).
2. Steady-state particle-front interaction in the period where the front approaches the particle to distances where intermolecular forces in the gap separating the particle from the front become significant [6,7]. Only recently have dynamic models for the interaction been presented and the manner in which engulfment/pushing is determined in steady-state analyses been re-examined [8–10].

There is some scattered work on examining the more realistic scenario of how non-planar solidification boundaries, particularly the ubiquitous dendritic fronts behave as they interact with embedded particles. There are few numerical simulations of the non-planar solidification front-particle interactions [8–10]. Wilde and Perepezko [11] have experimentally shown that in most circumstances, particles are more likely to get pushed at the beginning and then get "entrapped" by sidebranches of the dendrites. In that case, most particles will be concentrated around grain boundaries. Theoretical treatments of dendritic growth in the presence of small particles using the phase field approach indicates that the grain morphology can be seriously influenced by the particles and "dizzy dendrites" [12] can be formed. There is also some work by Kurien and Sasikumar [13] on the interaction of a growing dendrite with a particle but quantitative insights are lacking.

In this paper we seek to achieve the following objectives:

(1) A sharp-interface numerical methodology is advanced to account for the interaction between the phase boundary and the particle surface. The sharp interface capability allows for identification of the approach and contact of the front with the particle. The use of levelsets to define the interfaces facilitates treatment of such interactions.

(2) The response of a growing dendrite to the presence of a particle embedded in the melt is studied in a limited parameter space. The particle is held stationary, a restriction which is rather limiting from the point of view of MMC solidification but which, due to the simplicity afforded, turns out to be instructive nevertheless. The results for the system under consideration, i.e. an undercooled pure melt, reveal that for particles of the type used in MMCs (particle to melt conductivity ratio $\lambda = \frac{k_p}{k_l} < 1$) the dendrite navigates around the particle and the entrapment mode observed by Wilde and Perepezko is in fact the most probable outcome.

2. Formulation and computational approach

2.1. Governing equations

The configuration adopted in the calculations is shown in Fig. 1. The heat conduction equation in the melt, solid and particle regions are solved along with interface conditions applied on the solid-melt interface, and the melt-particle interface. The following characteristic scales are used to non-dimensionalize the governing equations: length scale $= X$, a characteristic length scale of the system (specified in Section 3), the time scale $= \frac{X^2}{\alpha_L}$, where α_L is the thermal diffusion coefficient, temperature scale $= T_S = \frac{H_{SL}}{\rho c_p}$, where H_{SL} is the latent heat of fusion per unit volume, ρ is the density of the liquid, and c_p is the specific heat of the liquid. The non-dimensional equations are then the following:

The energy equation in the melt and the solid phase (matrix material) is:

$$\frac{\partial \Theta}{\partial t} = \alpha^*_{L/S/P} \nabla^2 \Theta \tag{1}$$

where $\Theta = (T - T_m)/T_S$ is the non-dimensional temperature, α^* is the non-dimensional diffusion coefficients, and subscripts 'L', 'S' and 'P' indicate liquid, solid and particle respectively. The non-dimensional interface conditions are then:

$$V_N = \frac{k_L \cdot T_S}{H_{SL} \cdot \alpha_L} \cdot \left[\frac{k_S}{k_L} \cdot \left(\frac{\partial \Theta}{\partial n} \right)_S - \left(\frac{\partial \Theta}{\partial n} \right)_L \right] \tag{2}$$

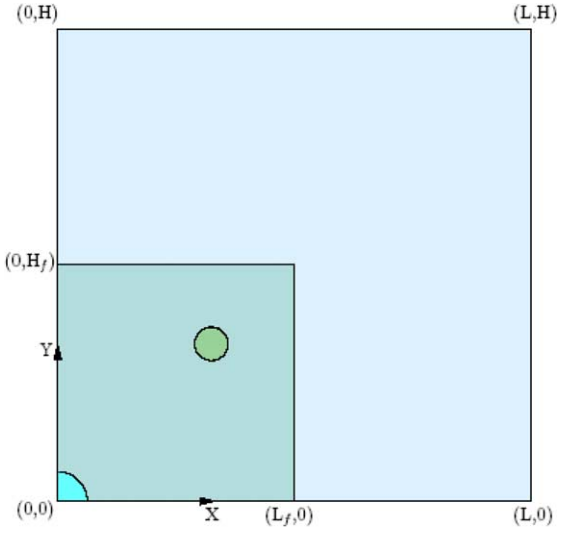

Fig. 1. Computational domain (L, H) has sub-domain (L_f, H_f) with fine mesh; particle is in the fine mesh sub-domain; the seed placed at (0, 0) grows into a dendrite.

We define a Stefan Number: $St = \frac{k_L \cdot T_S}{H_{SL} \cdot \alpha_L}$, and the non-dimensional interface temperature:

$$\Theta_{L,int} = -\Gamma(\theta)\kappa^* \tag{3}$$

where V_N, k_L, k_S, and κ^* are the non-dimensional velocity, liquid thermal conductivity, solid thermal conductivity, and non-dimensional curvature, respectively. The quantity $\Gamma(\theta) = \frac{\sigma_{sl} T_m}{H_{SL} \chi T_S}(1 - 15\varepsilon\cos(m(\theta - \theta_0))) = \gamma_0 f(\theta)$ is the non-dimensional capillarity parameter, σ_{sl} is the solid–liquid interfacial energy, θ is the angle with respect to the x-axis, parameter ε regulates the anisotropy strength and m the symmetry characteristics (i.e. $m = 4$ for fourfold symmetry) and θ_0 is the orientation of the preferred growth direction of the dendrite with the x-axis. $\Gamma_0 = \frac{\sigma_{sl} T_m}{H_{SL} T_S}$ is a capillary length and γ_0 is its non-dimensional counterpart. Note that the interfacial tension has a directional dependency, which reflects crystalline anisotropy [14,15].

The interface temperature of the particle-melt interface is determined by heat flux balance:

$$k_P \left(\frac{\partial \Theta}{\partial n}\right)_P = k_L \left(\frac{\partial \Theta}{\partial n}\right)_L \tag{4}$$

2.2. Computational technique

The computational approach is described in detail in [16]. A narrow-band levelset [17] is used to represent each of the embedded interfaces, i.e. the solidification front and the solid particle. The governing equations are discretized using the techniques described in [16]. The presence of the interfaces is accounted for by using the level-set field to redefine the discretization stencil at computational points that straddle the interface. This simplifies immensely the task of developing a sharp-interface methodology for complex interfaces, such as dendritic fronts. The methodology has been carefully benchmarked and the dendrites computed have been shown to match very well with theoretical predictions of tip characteristics from solvability theory.

2.3. Interfacial conditions

In computing the interaction of a dendrite with a stationary particle in the melt the key issue is how to deal with the interfacial conditions which can be of three types depending on the manner in which the dendrite approaches the particle: the solid–liquid interface of the metallic matrix, the particle-melt interface and the particle-solid interface (when the particle is contacted and engulfed by the solidifying front). In the present sharp interface approach these interfaces are maintained as sharp entities and defined by the zero-contours of the respective level-set fields. Thus, since the interfaces can be delineated interfacial conditions can be applied precisely on the interfaces. The normal and curvature values are computed from the levelset field [17] and stored on the Cartesian grid. The use of the level-set representation facilitates the application of such interface conditions as described below.

Eq. (3) is used to determine the interface temperature at the solid–liquid interface if there are no particles in the vicinity. In the discretization procedure [16], the temperature values are obtained at the locations indicated by the I_x and I_y in Fig. 2. These locations are obtained in a straightforward manner from the level-set information:

$$x_{I_x} = x_{i,j} + \Delta x_{I_x}, \quad y_{I_x} = y_{i,j} \tag{5a}$$

$$x_{I_y} = x_{i,j}, \quad y_{I_y} = y_{i,j} - \Delta y_{I_y} \tag{5b}$$

$$\frac{\Delta x_I}{\Delta x} \cong \left|\frac{(\phi_l)_{I_x} - (\phi_l)_{i,j}}{(\phi_l)_{i+1,j} - (\phi_l)_{i,j}}\right| = \left|\frac{0 - (\phi_l)_{i,j}}{(\phi_l)_{i+1,j} - (\phi_l)_{i,j}}\right|$$

$$\frac{\Delta y_I}{\Delta y} \cong \left|\frac{(\phi_l)_{I_y} - (\phi_l)_{i,j}}{(\phi_l)_{i,j} - (\phi_l)_{i,j-1}}\right| = \left|\frac{0 - (\phi_l)_{i,j}}{(\phi_l)_{i+1,j} - (\phi_l)_{i,j}}\right| \tag{5c}$$

where ϕ_l is a level-set field defined such that $\phi_l > 0$ in the liquid, <0 in a solid, and $=0$ on the interface, and Δx and Δy are the grid spacing in the x- and y-direction, respectively. The subscript l is an index representing the levelset number (for example, the solid–liquid interface may be defined as the first levelset, while the particle surface is defined by a second levelset). At any point defined by the coordinates given in Eq. (5) the interface temperature is then obtained from Eq. (3) (using the value of curvature bilinearly interpolated from the surrounding grid points).

The solid–liquid interface velocity is determined by the non-dimensional Stefan condition (Eq. (2)), where the normal gradients of the temperature $\left(\frac{\partial \Theta}{\partial n}\right)_{S/L}$ at the solid–liquid interface are obtained using normal probe

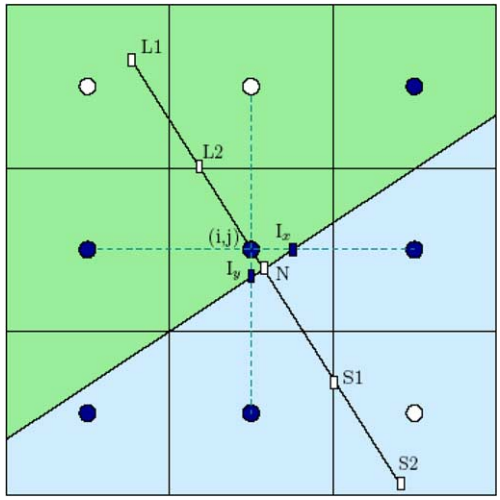

Fig. 2. Method for evaluating the normal gradients at the interface.

technique presented in detail in Yang et al. [16]. In the liquid phase, for example, the normal gradient of temperature (to second order accuracy) can be written as:

$$\left(\frac{\partial \Theta}{\partial n}\right)_{\mathrm{L}} = 2\Theta_{\mathrm{L1}} - \frac{1}{2}\Theta_{\mathrm{L2}} - \frac{3}{2}\Theta_{\mathrm{LI}} \tag{6}$$

For each of the *interfacial points* (i.e. points that straddle the interface) the interface velocity is computed at the locations denoted by N in Fig. 2. This location is given by:

$$\vec{x}_{\mathrm{N}} = \vec{x}_{i,j} - \vec{n}_{i,j}(\phi_I)_{i,j} \tag{7}$$

The locations of the probe points in liquid and solid phases can be calculated using the following:

$$\vec{x}_{\mathrm{L1}} = \vec{x}_{\mathrm{N}} + \vec{n}_{\mathrm{N}}\,\mathrm{d}x_{\mathrm{L1}} \tag{8a}$$

$$\vec{x}_{\mathrm{L2}} = \vec{x}_{\mathrm{N}} + \vec{n}_{\mathrm{N}}\,\mathrm{d}x_{\mathrm{L2}} \tag{8b}$$

$$\vec{x}_{\mathrm{S1}} = \vec{x}_{\mathrm{N}} - \vec{n}_{\mathrm{N}}\,\mathrm{d}x_{\mathrm{S1}} \tag{8c}$$

$$\vec{x}_{\mathrm{S2}} = \vec{x}_{\mathrm{N}} - \vec{n}_{\mathrm{N}}\,\mathrm{d}x_{\mathrm{S2}} \tag{8d}$$

Bilinear interpolation is performed from the surrounding mesh points to obtain the value of the variable Θ at points $\vec{x}_{\mathrm{L1}}$, $\vec{x}_{\mathrm{L2}}$, $\vec{x}_{\mathrm{S1}}$, $\vec{x}_{\mathrm{S2}}$. The normal vector at N, $\vec{n}_{\mathrm{N}}$ is also obtained by bilinear interpolation from the surrounding mesh points. The temperature gradient at the particle-melt interface $\left(\frac{\partial \Theta}{\partial n}\right)_{P/L}$ in Eq. (4) can be obtained in a similar way. Thus, the Stefan condition can be used to determine solid–liquid interface velocity and the heat balance condition can be used to obtain the temperature at the particle surface using the above conditions.

The simulations follow a dendrite as it grows towards, interacts with and engulfs a stationary particle in the melt. When the solidification front approaches close enough to the solid particle the two normal probe points required to extract gradient information in Eq. (6) may no longer lie in the liquid phase. Therefore, when contact between the solidification front and the particle is imminent special treatment is needed to update the motion of the solidification front. In the current framework, using the level-set information, it is a simple matter to detect when this type of situation arises. For example, once the probe point locations are determined (Eqs. (8a) and (8b)) for the solidification front on the liquid side, the value of the level-set defining the particle is computed at that point (using a bilinear interpolation) from the surrounding grid points. If the level-set value (for the particle) at that point happens to be negative then that probe point lies inside the particle and therefore is not available for computation of the gradient in Eq. (6). When only the second probe point P2 lies inside the particle but P1 lies in the liquid, then as demonstrated in Fig. 3(a), the gradient is obtained using only

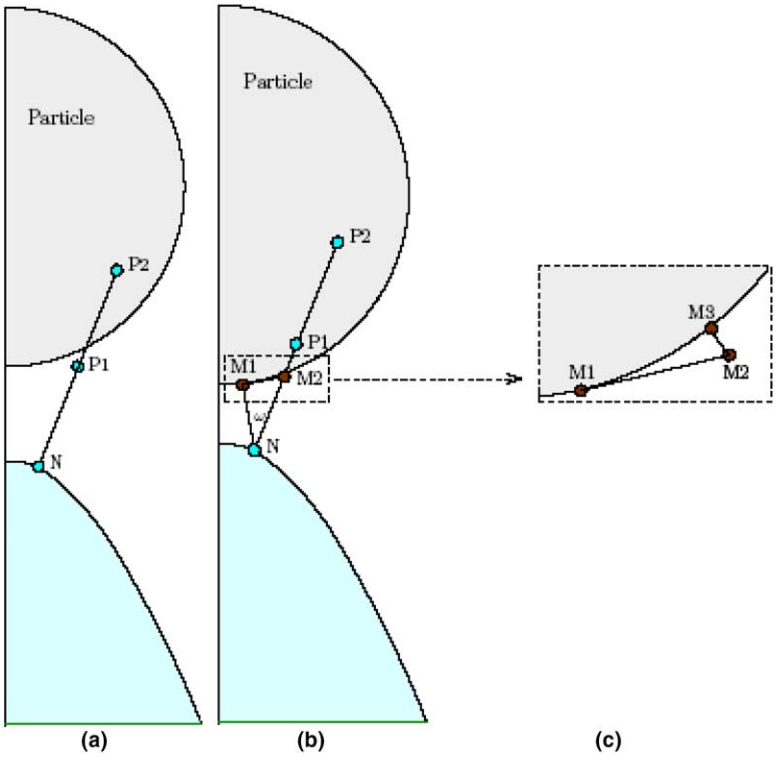

Fig. 3. (a) Second probe point is in a different phase, (b) first probe point is in a different phase and (c) amplified snapshot from (b).

one probe point in the liquid phase. This leads to a first order estimate for the gradient. In this case, only two points, i.e. the first probe P1 and interface point N are available for calculation of the temperature gradient. As the gap between the dendrite and the particle narrows and the first probe point P1 is also inside the particle, then contact is considered to have occurred, i.e. the gap between the front and particle is less than one grid spacing. Thus, the first probe point is now placed on the point M2 (Fig. 3(b)) which lies on the particle surface and the two interface points N and M2 are used to obtain the normal gradient of the temperature. The particle interface point M2 is located at:

$$\vec{x}_{M2} = \vec{x}_N + \vec{n}_N \, dx_{NM2} \tag{9}$$

where the distance dx_{NM2} is given by:

$$dx_{NM2} = \frac{(\phi_P)_N}{\cos\omega} \tag{10}$$

Where $(\phi_P)_N$ is the value of the distance function corresponding to the particle surface computed at the point N, i.e., the distance |M1N| as illustrated in Fig. 3(b), and ω, the angle $\angle$M1NM2 as illustrated in Fig. 3(b), is given by:

$$\omega = ATAN\left\{ABS\left[\frac{(n_y)_P}{(n_x)_P} - \frac{(n_y)_F}{(n_x)_F}\right]\right\} \tag{11}$$

In Eq. (11) $(n_{y/x})_P$ is the y/x component of the normal to the particle surface (i.e. computed from the level-set field defining the particle surface) computed at the solid–liquid interface point N. Similarly $(n_{y/x})_F$ is the y/x component of the normal to the solidification front computed at point N. In general, due to the curvature of the particle surface the point M2 will not lie exactly on the particle surface. Therefore the closest point on the particle surface, denoted M3 in Fig. 3(c) is identified and the temperature at that point is chosen as the particle surface temperature. This point M3 can be easily located (see illustration in Fig. 3(c)) using the following equation:

$$\vec{x}_{M3} = \vec{x}_{M2} + \vec{n}_{M2}(\phi_P)_{M2} \tag{12}$$

where $\vec{n}_{M2}$ is the normal at point M2 with respect to the particle interface.

The value of the temperature at the point M3 is obtained from the heat flux balance at the particle surface. This is described below.

The solid–liquid interface is taken to be in perfect thermal contact in the situation illustrated in Fig. 3(b). Therefore, when the gap between the phase boundary and the particle is less than a grid spacing the temperature at point N is taken to be equal to that at the point M3. Then, the following conditions are satisfied:

$$\Theta_N = \Theta_{M3} \tag{13}$$

and heat flux balance:

$$k_P\left(\frac{\partial\Theta}{\partial n}\right)_P = k_S\left(\frac{\partial\Theta}{\partial n}\right)_S \tag{14}$$

In discrete form the above equation is

$$k_P\left(2\Theta_{P1} - \frac{1}{2}\Theta_{P2} - \frac{3}{2}\Theta_{M3}\right) = k_S\left(2\Theta_{S1} - \frac{1}{2}\Theta_{S2} - \frac{3}{2}\Theta_N\right) \tag{15}$$

Using Eq. (13):

$$\Theta_N = \Theta_{M3} = \frac{4(k_S\Theta_{S1} - k_P\Theta_{P1}) - (k_S\Theta_{S2} - k_P\Theta_{P2})}{3(k_S - k_P)} \tag{16}$$

Here the values of temperature in the particle and solid, i.e. Θ_{P1}, Θ_{P2} and Θ_{S1}, Θ_{S2} respectively are again computed using bilinear interpolation from the surrounding grid points.

3. Results

3.1. Computational setup

The computational domain (of extent $L \times H$ units, where $L = H = 10$) is shown in Fig. 1. The length scale here was chosen to correspond to typical dendritic tip radius scales (and to typical particle size ranges in metal-matrix composites). Therefore $X = 1000\Gamma_0$ was chosen where Γ_0 is the capillary length. Therefore the tip radius in this scale is order 1 and the simulations performed below can be viewed as representing interactions between dendrites and particles of radii comparable to the dendrite tip radius. This amounts to particles in the micron to 10 micron range for commonly used phase change materials (such as succinonitrile). A sub-domain ($L_f \times H_f$, where $L_f = H_f = 4$) has fine mesh with a fixed particle in it. The mesh density (400×400 in fine mesh sub-domain) employed for the calculations was chosen based on grid refinement studies and on the convergence studies for dendritic growth presented in [16]. The melt is initially uniformly undercooled and a seed crystal is placed at the origin as shown in Fig. 1, which eventually grows to form a dendrite. Symmetry boundary conditions are set at the left and the bottom boundaries. The temperatures of the upper and the right boundaries are fixed at the undercooling temperature. This setup is used to perform the numerical simulations of the dendritic solidification in the presence of the embedded particle. The results are obtained below for solidification using different particle sizes, dendrite orientation, strength of solid–liquid interfacial energy (i.e. dendrite tip radius and velocity) and particle to melt conductivity ratio λ. In each case an undercooling of $\Delta = -0.55$ is imposed on the boundaries and the initial melt. Note

that this undercooling is high in comparison to practical crystal growth conditions.

Fig. 4 shows the interaction of a dendrite with a particle (of radius 0.4) embedded in the melt. In this case the growth parameters are $\gamma_0 = 0.000925$, $\varepsilon = 0.1$, $\theta_0 = 45°$, $\lambda = 0.01$. To examine the most general situation the dendrite has been allowed to grow in a direction that leads to an interaction that is not head-on with the particle. The value of particle to melt conductivity ratio ($\lambda = 0.01$) chosen corresponds to a typical Aluminium-Silica metal-matrix composite. It is observed that the dendrite grows in the specified growth direction, establishes a steady-state tip velocity and radius and approaches the particle unhindered until the thermal boundary layer contacts the particle. In the case shown in Fig. 4, i.e. when $\lambda < 1$, the presence of a particle of poor conductivity causes the dendrite to deform and navigate around the obstruction to heat flow. From the point of view of solidification, this is expected, since the dendrite will grow in the direction of largest heat flux and the particle discourages heat flow through it. However, from the viewpoint of particle-front interaction theory this result is interesting. Almost all analyses of particle-front interactions deal with planar (non-dendritic) solid–liquid fronts approaching a particle in idealized and controlled growth conditions (such as directional solidification in small samples). According to fairly well established planar front-particle interaction theory [4,6–9], in the case where $\lambda < 1$ the particle should get pushed ahead by the front. This is due to the shape assumed by the planar interface as it approaches the particle in the directional solidification setting and the resulting intermolecular repulsion forces that tend to push the particle away from the front. This repulsive force is opposed by a hydrodynamic drag force primarily arising from the flow of melt in the gap between the front and the particle. However, provided the repulsive interaction between the particle and the front is strong

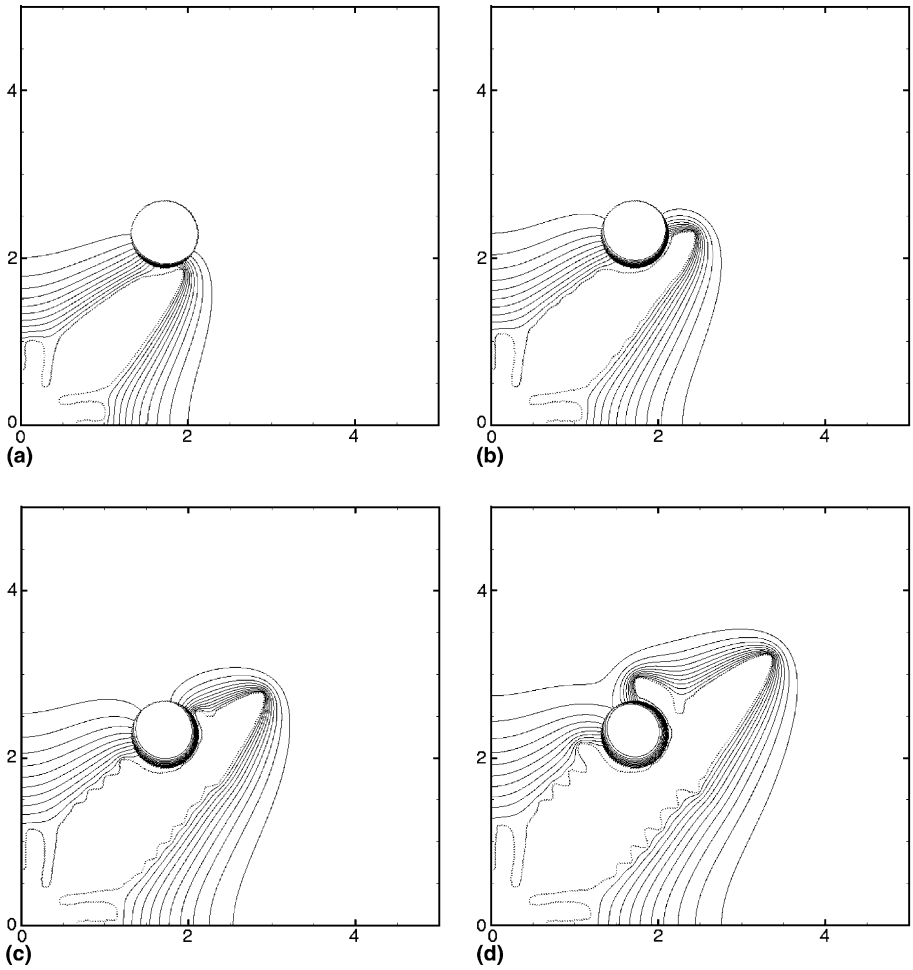

Fig. 4. Solid–liquid interface shape when interacting with embedded particle with: $\lambda = 0.01$, $R_P = 0.4$. Time interval $\Delta t = 0.03$.

enough to overcome the restoring drag force the particle will move away from the front. Conversely, for typical systems, when $\lambda > 1$ the particle will be "engulfed" by the planar solid–liquid interface. These scenarios of particle-front interactions are experimentally observed and theoretically justifiable in directional solidification systems in pure materials [18,19]. For practical solidification processes such as castings, whether for pure materials or otherwise, where: (1) the planarity of the interface cannot be maintained and the cellular/dendritic growth regimes are the norm, and (2) the somewhat restrictive heat flow conditions applicable to the directional solidification system do not exist conclusions from particle-front interaction theory regarding pushing/engulfment may not be applicable. In fact, under such growth conditions, the "entrapment" mode of particle-front interaction may be more likely [11]. This third mode of interaction implies that the particles are trapped between the sidebranches of dendrites and upon completion of solidification are typically segregated at grain boundaries. There is however little theoretical understanding of the interaction of non-planar fronts with

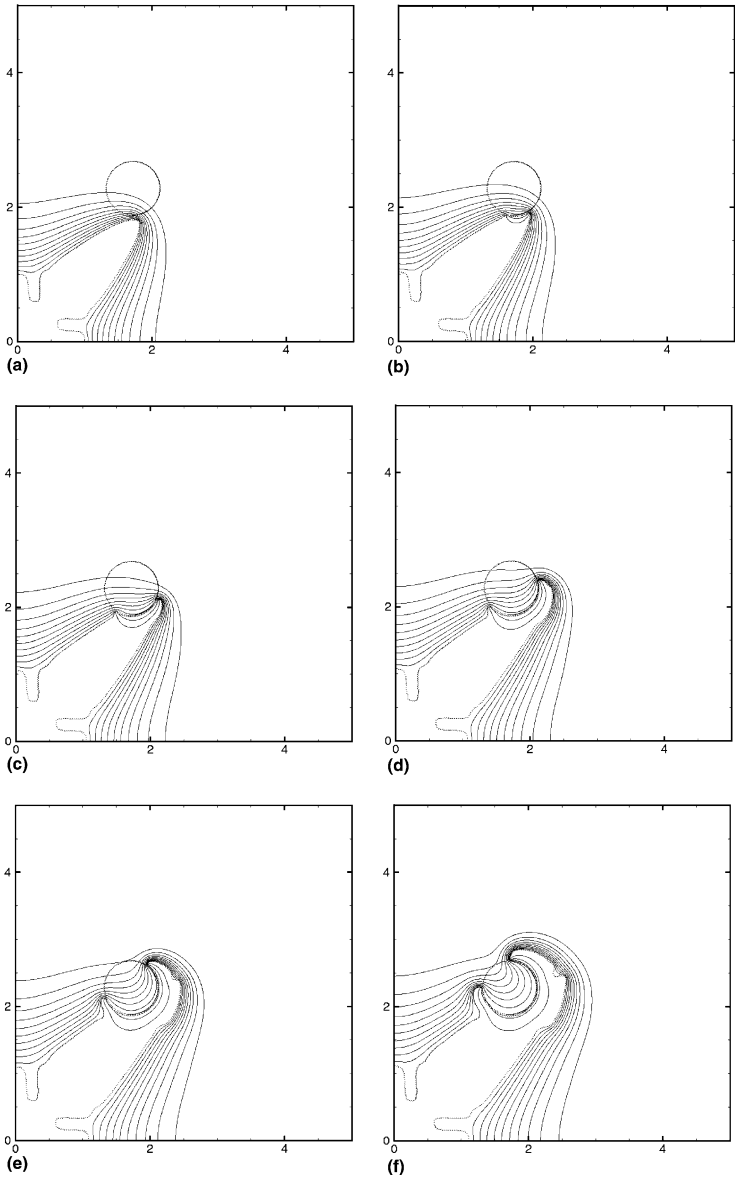

Fig. 5. Solid–liquid interface shape when interacting with embedded particle with: $\lambda = 1$, $R_P = 0.4$. Time interval $\Delta t = 0.03$.

particles in the melt in a general solidification setting. In this context the present simulations offer useful insights as discussed below.

In particle-front interaction theory pertaining to a planar interface approaching an initially stationary particle, the pushing/engulfment/entrapment behaviour is determined by the strength of the intermolecular (van der Waals [6]/disjoining pressure [20]) interactions between the solid and the particle across a melt gap. This melt gap needs to be of the order of the interaction length scales (typically tens of nanometers [7,21]) for the interactions leading to pushing to occur. In the case shown in Fig. 4 however, the solid–liquid interface in fact can not get close enough to the particle to activate the particle pushing mechanism. The front chooses to go around the particle and finally the particle gets "entrapped" by sidebranches. The Fig. 4(a)–(d) show the progression of the dendrite around the particle. In these figures, the circle represents the particle, the dotted line represents the shape of the dendrite tip and the solid lines represent the isothermal contours in front of the dendrite tip. It is noticed that when the front is approaching the particle a pool of melt of significant thickness forms between the front and the particle thereby slowing the contact between the solid–liquid interface and the particle. Therefore, it is likely that, at least under the present growth scenario leading to dendritic growth in a pure material, the dendritic tip as well as the sidebranches of the dendrite will encircle the particle even before the pushing interaction can be activated.

For particle-melt thermal conductivity ratio $\lambda \geqslant 1$, the scenario is different. Fig. 5 shows the process of the interaction of solid–liquid interface with $\lambda = 1$ and other parameters the same as for Fig. 4. In this case, since the particle and melt properties are the same the dendrite does not feel the particle prior to approach.

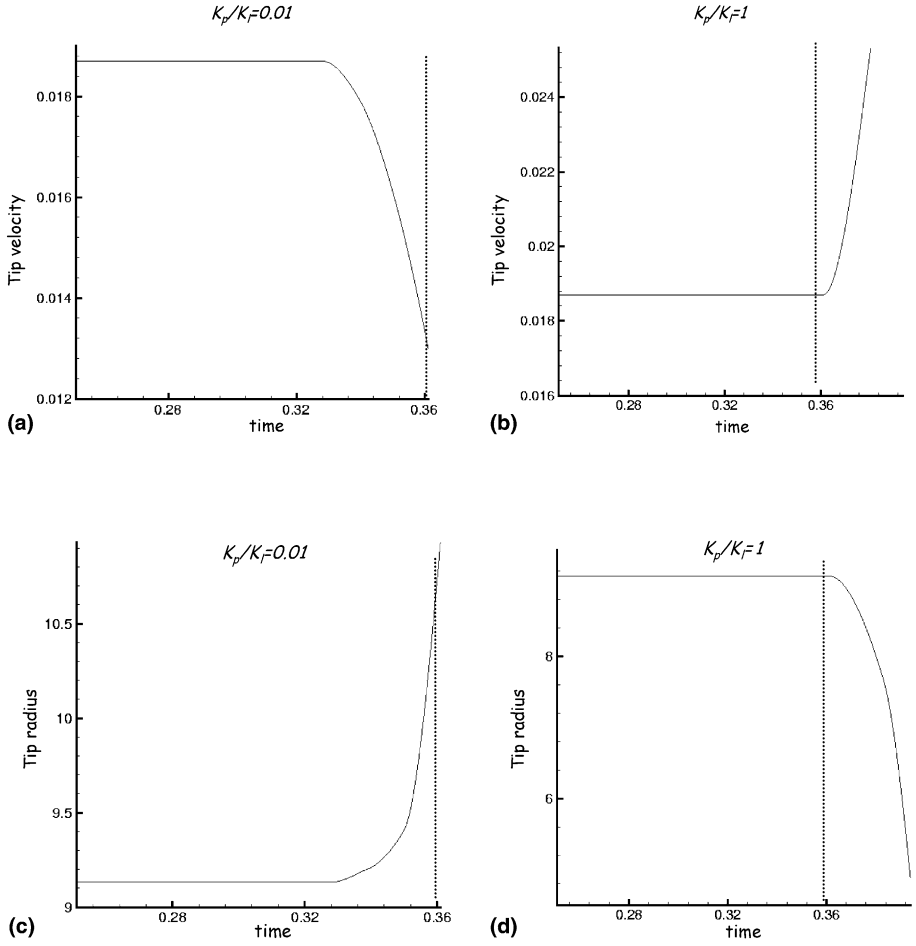

Fig. 6. Tip characteristics of a dendrite as it approaches the particle. The vertical dotted line shows the time of contact between the particle and the dendrite. (a) Dendrite tip velocity against time for $\lambda = 0.01$, (b) dendrite tip velocity against time for $\lambda = 1$, (c) dendrite tip radius against time for $\lambda = 0.01$, (d) dendrite tip radius against time for $\lambda = 1$.

In fact, here the "contact" conditions (Eq. (13)) between the dendrite and the particle are called into play. This is clearly seen from the isotherm contours in Fig. 5(a)–(f). The contours run smoothly through the particle and no preferred heat flow direction is established for the dendrite. In fact, in this case the presence of the particle, after contact appears to homogenize the heat flow and the front wraps around the particle in a nearly uniform fashion as it continues to solidify. The solidification front therefore adjusts its shape to fit the particle shape until it finally encloses the particle. Further growth then ensues with a newly formed tip that will continue to grow in the preferred growth direction (due to interfacial energy anisotropy).

For the cases in Figs. 4 and 5, the dendrite tip velocity and tip radius are recorded before the solid–liquid interface hits the particle and thereafter. The tip velocity (Fig. 6(a)), for the case with $\lambda = 0.01$ drops as the front approaches the particle. This retardation is because the particle hinders heat flow through it. The time when the dendrite begins to interact with the particle corresponds to the drop in velocity and increase in tip radius (Fig. 6(c)). The dotted vertical line shows the time when the solid–liquid front has begun to navigate around the particle. After this point (corresponding to 4(a)) it is difficult to identify a "tip" for the dendrite until it has crossed the particle and has recovered to a symmetric steady-state shape again (as in Fig. 4(d)). For $\lambda = 1$, on the contrary, the dendrite tip velocity remains unaffected as it approaches the particle and contacts it at the instant marked by the vertical dotted line in Fig. 6(b). Following the contact the leading part of the solidification front rapidly wraps around the particle (as seen by the steep increase in the velocity of the leading point of the front). This is because the solidification front assumes a sharp tip after contact and therefore travels rapidly around the particle.

Fig. 7 shows a detailed view of the region of interaction of the dendrite with the particle. Fig. 7(a) shows the dendrite tip and particle in the region of interaction (see Fig. 4(a)) for $\lambda < 1$. The presence of a film of melt between the solid–liquid front and the particle is seen in the figure. Also shown in the figure are the isotherms. Clearly the melt pool between the particle and front is a region of relatively warm fluid and small temperature gradients. This pool will therefore solidify rather slowly. The higher temperature gradients are away from the interface and drive the trip around the particle. There are still sufficient mesh points that resolve the film. In the case of $\lambda = 1$, i.e. as shown in Fig. 5, the solid–liquid interface and the particle are in "contact", i.e. there is no liquid film that remains between the interfaces and the zero-levelsets corresponding to the two interfaces are less than one mesh cell apart. The contact condition (Eq. (13)) is imposed at the solid–liquid and particle-melt interface that are less than a mesh cell apart, (i.e. we consider that the solidification front has perfect thermal contact with the particle).

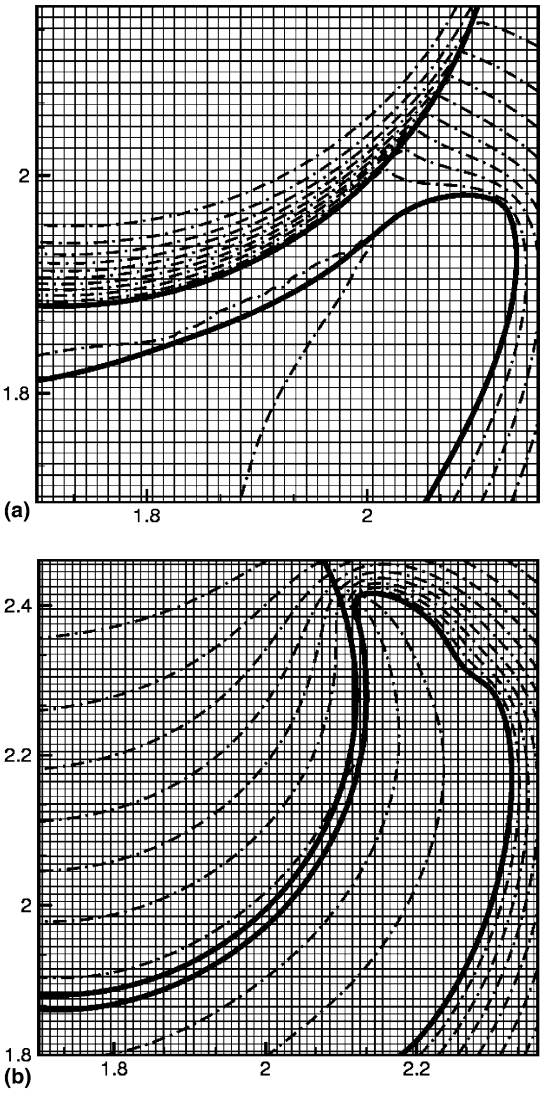

Fig. 7. Zoomed in view of the solid–liquid interface shape when interacting with embedded particle. (a) For the situation shown in Fig. 4(a), $\lambda = 0.01$. (b) For the situation shown in Fig. 5(c), $\lambda = 1.0$.

Figs. 8 and 9 show the interaction of a dendrite with a particle placed in the melt, the difference in the two cases being the particle radius. In Fig. 8 the particle radius is 0.2 while in Fig. 9 it is 0.1. Other parameters are $\gamma_0 = 0.000625$, $\varepsilon = 0.1$, $\theta_0 = 45°$, $\lambda = 0.1$. Figs. 8(a) and 9(a) show the evolution of interface shapes as the dendrite grows around the particle. Figs. 8(b)–(e) and 9(b)–(e) show the isotherms during the evolution of the interface. The sidebranching activity in this case is enhanced due to the smaller surface tension used in these

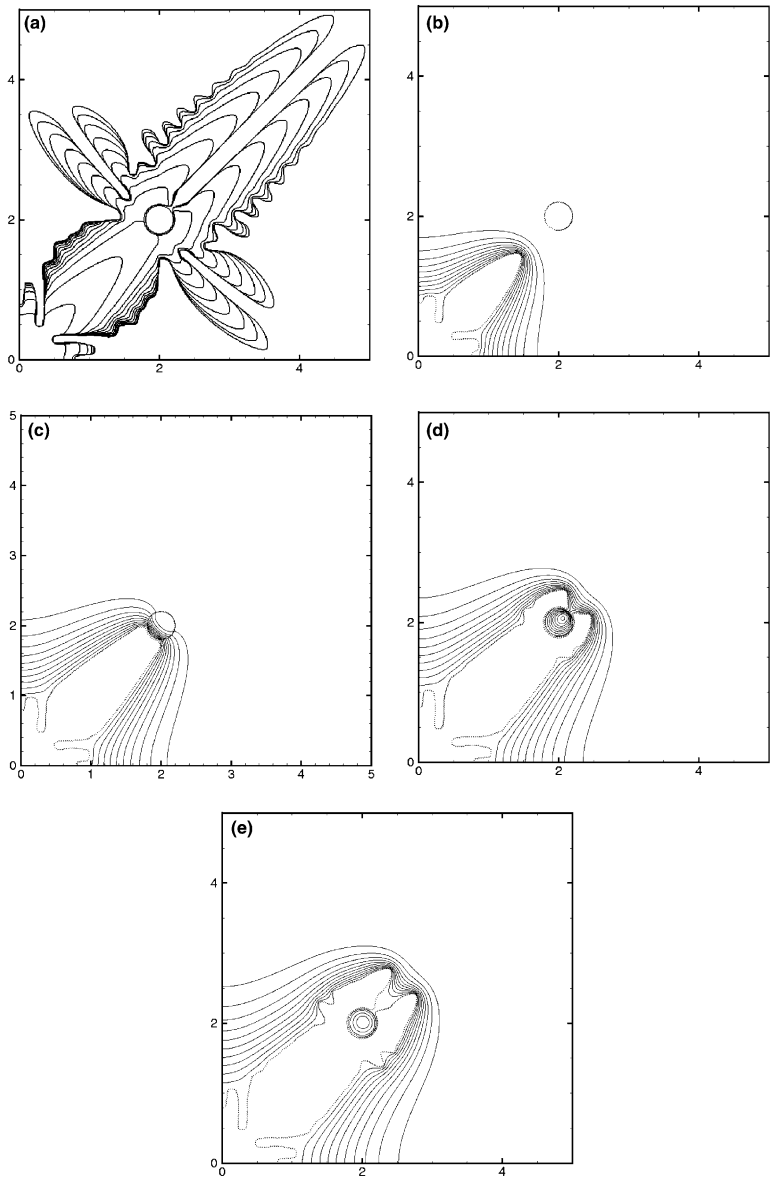

Fig. 8. Dendrite-particle interaction with particle of radius $R_P = 0.2$, thermal conductivity ratio $\lambda = 0.1$, capillarity parameter $\gamma_0 = 0.000625$, (a)–(e) time interval $\Delta t = 0.03$.

cases when compared to Figs. 4 and 5. In each case the tip of the primary dendrite is split by the particle and leads, in this 2-dimensional case to the further progression of two independent tips which are separated by a groove of melt. It is seen that the smaller the particle, the less intense the sidebranching caused by the particle because the tip is less disturbed by the particle. It is also observed that the pool of melt surrounding the particle is narrower for the smaller particle for the same reason. Therefore the possibility that the repulsive interactions responsible for particle pushing will occur is perhaps higher for the smaller particles than for the larger particle. In general, even for planar fronts small particles are more likely to be pushed than larger ones [4].

Figs. 10 and 11 compare the effect of increasing the thermal conductivity ratio for a particle of radius 0.2 approached by a dendrite. In these cases $\gamma_0 = 0.0025$, $\varepsilon = 0.1$, $\theta_0 = 0°$. For the case in Fig. 10 $\lambda = 1$ while in Fig. 11 $\lambda = 10$. In Fig. 10 the dendrite does not see the particle until contact. Following contact the dendrite resumes formation of parabolic tips. The presence of the circular particle homogenizes the heat flow directions

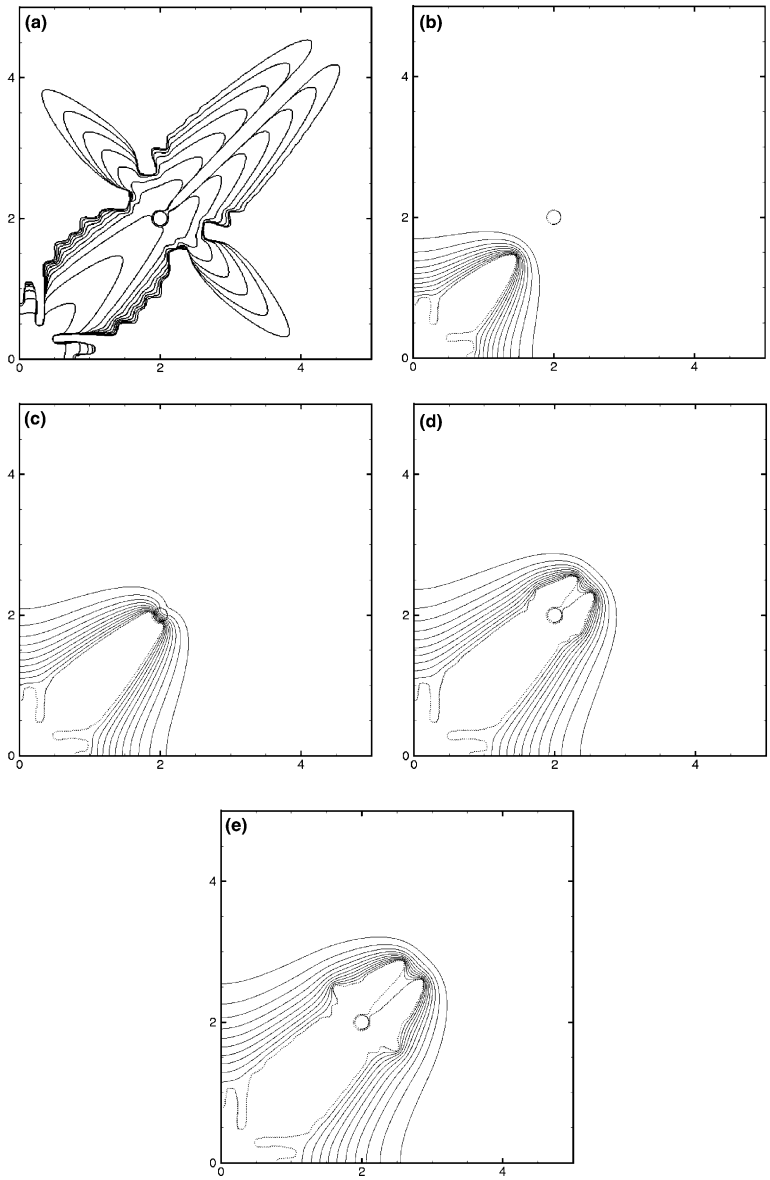

Fig. 9. Dendrite-particle interaction with particle of radius $R_P = 0.1$, thermal conductivity ratio $\lambda = 0.1$, capillarity parameter $\gamma_0 = 0.000625$, (a)–(e) time interval $\Delta t = 0.03$.

after contact however and two mutually perpendicular tips arise due to the fourfold crystalline anisotropy. Note that prior to contact with the particle, as in Fig. 10(b) the heat flow is transparent to the presence of the particle. In the case of $\lambda = 10$, shown in Fig. 11, the presence of the particle in effect accelerates the dendrite tip as it approaches the particle. In this case the dendrite tip contacts the particle in a manner similar to that for $\lambda = 1$. A key observation in these cases is that the curvature of the solid–liquid interfaces for all of the above simulations, i.e. for the range of $0.01 < \lambda < 10$ is opposite in sign to the curvatures for the directional solidification cases. The curvature of the interface (due to the influence of λ) has a significant effect on the pushing/engulfment behaviour of particles. Therefore it remains to examine what implication the reversal of the sign of curvature in the current undercooled melt simulations (in comparison with previous directional solidification studies) will have on particle-front interactions. The present study focussed on developing the ability to compute the interaction of a dendrite with a particle using a sharp-interface technique. In future work the

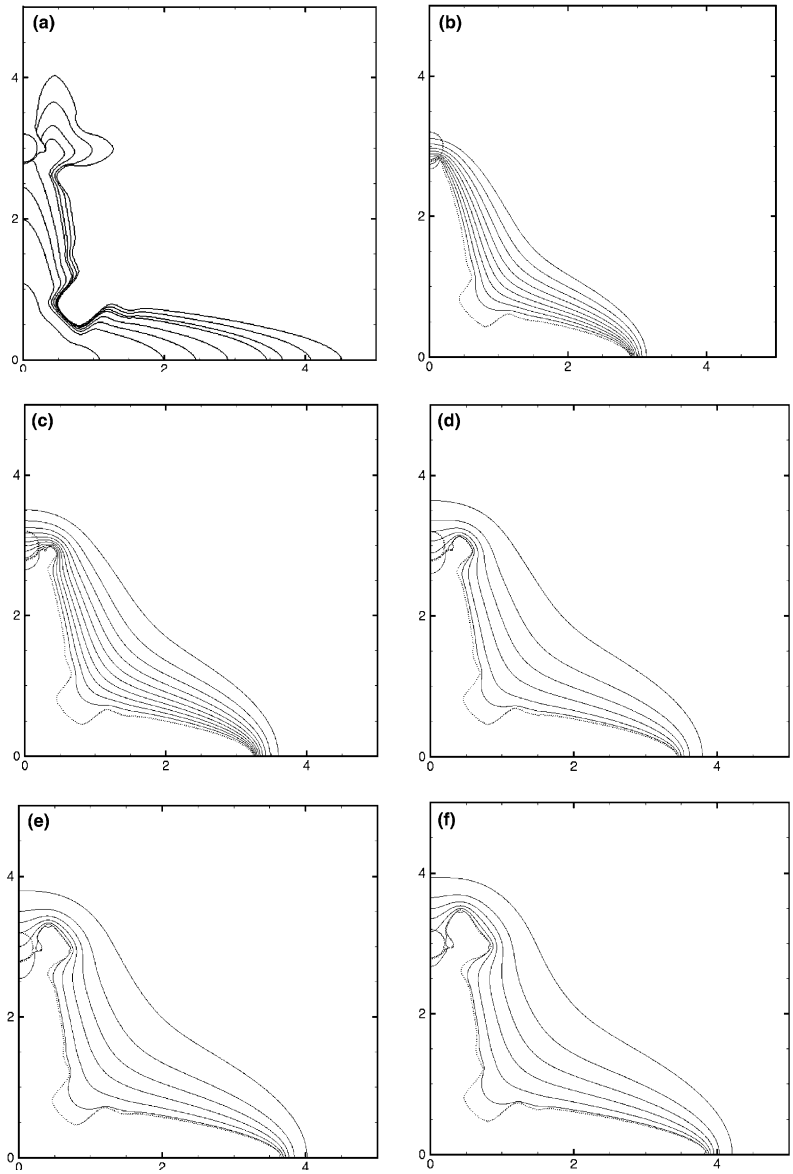

Fig. 10. Dendrite-particle interaction with particle of radius $R_P = 0.2$, thermal conductivity ratio $\lambda = 1$, capillarity parameter $\gamma_0 = 0.0025$, (a)–(f) time interval $\Delta t = 0.03$.

dynamics of the particle due to the forces acting between it and the solid–liquid interface will be included to examine the coupling between dendrite growth and particle motion during dendrite-particle interactions.

4. Summary

A sharp interface level-set based method is presented for the numerical simulations of interaction of dendritic fronts with stationary particles in the melt. The use of levelsets to define and track interfaces facilitates maintaining sharp interacting interfaces, and treatment of contact between the interfaces. A limited region of parameter space has been covered in this paper. The dendrites were grown in an undercooled pure melt. This system is different from that typically employed in particle-front interaction theory and experiment where directional solidification is employed to control interfacial motion. In such cases the planarity of the interface is sought to be maintained and much of the theory of particle-front interactions therefore

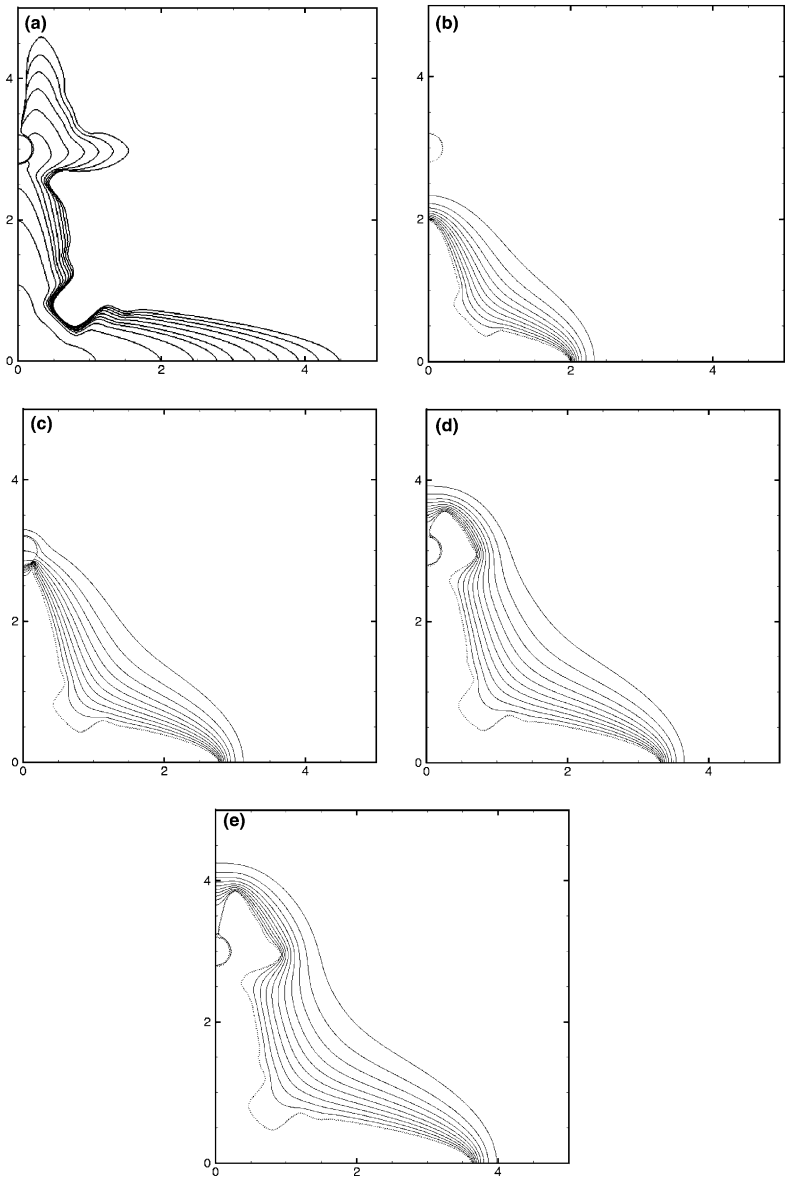

Fig. 11. Dendrite-particle interaction with particle of radius $R_P = 0.2$, thermal conductivity ratio $\lambda = 10$, capillarity parameter $\gamma_0 = 0.0025$, (a)–(e) time interval $\Delta t = 0.03$.

has been developed in that setting. In the scenario explored in this paper, where unstable (dendritic) fronts interact with the particle rather than stable (planar) fronts conclusions from particle-front interaction theory may not apply. In particular, the current results indicate that for undercooled melts and a particle to melt conductivity ratio $\lambda < 1$ the dendrite tends to navigate around the particle and a melt pool is formed between the particle and the front. The closure of the melt pool occurs over a time that is long compared to that required for the dendrite to "entrap" the particle within its sidebranches. In the cases studied the tip velocity and curvature of the dendrite and hence the manner in which it interacts with the particle is determined by the value of λ. For $\lambda < 1$ the tip is decelerated by the particle; for $\lambda = 1$ the tip does not feel the particle; for $\lambda > 1$ the tip is accelerated by the particle. These responses are reversed with respect to the situation typically employed in particle-front analyses of directional solidification and planar fronts. Interactions of dendrites with particles that are free to move in the melt will be further examined in future work.

Acknowledgements

This work was supported by a National Science Foundation CAREER Award (CTS-0092750) to the third author.

References

[1] S.N. Omenyi, A.W. Neumann, Thermodynamic aspects of particle engulfment by solidifying melts, J. Appl. Phys. 47 (9) (1976) 3956–3962.
[2] G.F. Bolling, J. Cissé, A theory for the interaction of particles with a solidifying front, J. Cryst. Growth 10 (1971) 56–66.
[3] D.R. Uhlmann, B. Chalmers, K.A. Jackson, Interaction between particles and a solid–liquid interface, J. Appl. Phys. 35 (1964) 2986–2993.
[4] R. Asthana, S.N. Tewari, Review the engulfment of foreign particles by a freezing interface, J. Mater. Sci. 28 (1993) 5414–5425.
[5] J. Pötschke, V. Rogge, On the behaviour of foreign particles at an advancing solid liquid interface, J. Cryst. Growth 94 (1989) 726–738.
[6] D.K. Shangguan, S. Ahuja, D.M. Stefanescu, An analytical model for the interaction between an insoluble particle and an advancing solid/liquid interface, Metall. Mater. Trans. A: Phys. Metall. Mater. Sci. 23 (A) (1992) 669–680.
[7] A.W. Rempel, M.G. Worster, The interaction between a particle and an advancing solidification front, J. Cryst. Growth 205 (1999) 427–440.
[8] J.W. Garvin, H.S. Udaykumar, Particle-solidification front dynamics using a fully coupled approach, Part I: methodology, J. Cryst. Growth 252 (1–3) (2003) 451–466.
[9] J.W. Garvin, H.S. Udaykumar, Particle-solidification front dynamics using a fully coupled approach, Part II: comparison of drag expressions, J. Cryst. Growth 252 (1–3) (2003) 467–479.
[10] A.V. Catalina, D.M. Stefanescu, S. Sen, Numerical calculation of the morphology of a solid/liquid interface near an insoluble particle, in: D.M. Stefanescu, J. Warren, M. Jolly, M. Krane (Eds.), Modeling of Casting, Welding, and Advanced Solidification Processes X, Sandestin Resort & Conference Center, Destin, Florida, 2003, pp. 125–132.
[11] G. Wilde, J.H. Perepezko, Experimental study of particle incorporation during dendritic solidification, Mater. Sci. Eng. A: Struct. Mater. Prop. Microstruct. Process. 283 (1–2) (2000) 25–37.
[12] L. Gránásy, T. Pusztai, J.A. Warren, J.F. Douglas, T. Börzsönyi, V. Ferreiro, Growth of 'dizzy dendrites' in a random field of foreign particles, Nature Mater. 2 (2003) 92–96.
[13] L. Kurien, R. Sasikumar, Simulation of dendrite morphology in the presence of particles, Acta Mater. 44 (8) (1996) 3385–3395.
[14] A. Karma, W.J. Rappel, Quantitative phase-field modeling of dendritic growth in two and three dimensions, Phys. Rev. E 57 (4) (1998) 4323–4349.
[15] Y.T. Kim, N. Goldenfeld, J. Dantzig, Computation of dendritic microstructures using a level set method, Phys. Rev. E 62 (2) (2000) 2471–2474.
[16] Y. Yang, H.S. Udaykumar, Sharp interface Cartesian grid method III: Solidification of pure materials and binary solutions, J. Comput. Phys. 210 (1) (2005) 55–74.
[17] J.A. Sethian, Level Set Methods and Fast Marching Methods: Evolving Interfaces in Computational Geometry, Fluid Mechanics, Computer Vision, and Materials Science, second ed., Cambridge University Press, 1999, pp. 77–84.
[18] D.M. Stefanescu, F.R. Juretzko, B.K. Dhindaw, A. Catalina, S. Sen, P.A. Curreri, Particle engulfment and pushing by solidifying interfaces, Part II: Microgravity experiments and theoretical analysis, Metall. Mater. Trans. A: Phys. Metall. Mater. Sci. 29 (A) (1998) 1697–1706.
[19] A.A. Chernov, D.E. Temkin, A.M. Mel'nikova, The influence of the thermal conductivity of a macroparticle on its capture by a crystal growing from a melt, Sov. Phys. Crystallogr. 22 (6) (1977) 656–658.
[20] J.G. Dash, H. Fu, J.S. Wettlaufer, The premelting of ice and its environmental consequences, Rep. Progr. Phys. 58 (1995) 115–167.
[21] J.N. Israelachvili, Intermolecular and Surface Forces, second ed., Academic Press, 1991.